Connexin Mutations Causing Skin Disease and Deafness Increase Hemichannel Activity and Cell Death when Expressed in *Xenopus* Oocytes

Jack R. Lee[1], Adam M. DeRosa[1] and Thomas W. White[1]

Mutations in the GJB2 gene-encoding connexin 26 (Cx26) have been linked to skin disorders and genetic deafness. However, the severity and type of the skin disorders caused by Cx26 mutations are heterogeneous. Here we explored the effect of Cx26 KID syndrome-associated mutations, G12R, S17F, and D50N on channel function. The Cx26 N14K mutation was also examined that is associated with deafness but has a skin disorder distinct from the KID syndrome mutations. The proteins were all expressed in *Xenopus* oocytes with levels equal to wild-type Cx26. The G12R, N14K, and D50N mutations resulted in larger hemichannel currents than the wild-type-expressing cells, but the S17F mutation resulted in a complete loss of hemichannel activity. Elevated hemichannel activity correlated with an increased cell death. This result could be reversed through the elevation of calcium (Ca^{2+}) in the extracellular media. Functional gap junctions were only produced by paired N14K cells, which had a similar conductance level to wild type, even though they exhibited a complete loss of voltage sensitivity. This set of data confirms that aberrant hemichannel activity is a common feature of Cx26 mutations associated with KID syndrome, and this may contribute to a loss of cell viability and tissue integrity.

Journal of Investigative Dermatology (2009) **129,** 870–878; doi:10.1038/jid.2008.335; published online 6 November 2008

INTRODUCTION

Mutations in connexin genes are associated with diverse hereditary human diseases (White and Paul, 1999; Wei *et al.*, 2004; Anand and Hackam, 2005; Mese *et al.*, 2007). Sensorineural hearing loss (SNHL) is the most common connexin-related disease that can be either nonsyndromic, or syndromic, when associated with skin disorders and other ectodermal abnormalities (Gerido and White, 2004; van Steensel *et al.*, 2004; Richard, 2005; Lai-Cheong *et al.*, 2007). SNHL is commonly linked to mutations in the Cx26-encoding gene GJB2 (Petit, 2006). Although mutations in Cx26 have been linked to a few rare autosomal dominant cases of nonsyndromic deafness (DFNA3), autosomal recessive mutations account for the vast majority of nonsyndromic hearing loss associated with GJB2 (DFNB1; Petit *et al.*, 2001). There is abundant evidence to suggest that loss-of-function mutations in Cx26 lead to generation of deafness, but not skin disease (White, 2000; Bruzzone *et al.*, 2003; Zhao *et al.*, 2006). In fact, the most common mutation, 35delG, produces a frame shift and early protein truncation in the N terminus and accounts for up to 85% of all the mutant GJB2 alleles in nonsyndromic deaf populations in Europe (Petit *et al.*, 2001).

Syndromic mutations in Cx26 are associated with a variety of skin disorders such as Vohwinkel syndrome, Bart–Pumphrey syndrome, palmoplantar keratoderma, or keratitis (and hystrix-like) ichthyosis deafness syndrome (KID/HID) and always present with autosomal dominant inheritance (Gerido and White, 2004; van Steensel *et al.*, 2004; Richard, 2005; Lai-Cheong *et al.*, 2007) The lack of associated skin disorders in cases of nonsyndromic SNHL shows that the function and development of the epidermis is not affected by the simple loss of Cx26 function as in the case of homozygous 35delG patients. Thus, the Cx26 mutations that can cause syndromic deafness associated with skin disease must show some type of alteration of function, but the mechanisms whereby Cx26 mutation leads to pathological changes in the epidermis remain to be elucidated.

Six connexin subunits oligomerize to form a hemichannel (Goodenough and Paul, 2003). A functional gap junction is formed when two plasma membrane hemichannels from adjacent cells align and create a direct communication pathway between their cytoplasms (Harris, 2001). Each connexin subunit is comprised of four transmembrane domains connected by two extracellular and one intracellular loop domains, containing cytoplasmic C and N termini. Historically, the formation of complete gap junction channels was thought to be the primary function of connexin subunits, although recently nonjunctional hemichannels have been speculated to

[1]*Department of Physiology and Biophysics, Stony Brook University Medical Center, Stony Brook, New York, USA*

Correspondence: Dr Thomas W. White, Department of Physiology and Biophysics, Stony Brook University Medical Center, T5-147, Basic Science Tower, Stony Brook, New York 11794-8661, USA.
E-mail: thomas.white@sunysb.edu

Abbreviations: HID, hystrix-like ichthyosis deafness syndrome; KID, keratitis ichthyosis deafness syndrome; MB, modified Barth's medium; SNHL, sensorineural hearing loss

Received 4 June 2008; revised 26 August 2008; accepted 4 September 2008; published online 6 November 2008

play a role in cellular homeostasis under different physiological conditions (Bennett *et al.*, 2003; Saez *et al.*, 2005).

As hemichannels may contribute to normal cell function, disease causing connexin mutations could also mediate their effects through alteration of hemichannel activity. Analysis of connexin mutations causing syndromic SNHL associated with skin disease has supported this idea. Examples include the A40V and G45E mutations of Cx26, both of which cause severe forms of KID syndrome, producing neonatal fatality in the case of G45E (Montgomery *et al.*, 2004; Janecke *et al.*, 2005; Jonard *et al.*, 2008). Both of these mutations displayed aberrant hemichannel activity leading to cell death *in vitro*, and constitutively active hemichannels was suggested to be the cause of the resultant epidermal pathology (Montgomery *et al.*, 2004; Stong *et al.*, 2006; Gerido *et al.*, 2007). These observations suggested that abnormal hemichannel activity may be a general feature of Cx26 mutations associated with KID/HID disorders.

Four additional Cx26 mutations G12R, N14K, S17F, and D50N have also been linked to cases of KID/HID syndrome (Richard *et al.*, 2002; van Geel *et al.*, 2002; van Steensel *et al.*, 2004; Mazereeuw-Hautier *et al.*, 2007). All patients exhibited SNHL symptoms, but the accompanying skin disorders varied in both clinical features and severity. KID/HID disorders cover a broad clinical spectrum, although several subtypes can be distinguished based on prevailing clinical features (Mazereeuw-Hautier *et al.*, 2007). However, there is not yet sufficient data to establish clear genotype–phenotype correlations, or to associate specific reported Cx26 mutations with distinct subtypes.

The functional properties of G12R, N14K, S17F, and D50N were characterized using an *in vitro* expression assay comprised of cRNA-injected *Xenopus* oocytes. All four mutations displayed significantly different membrane currents than wild-type Cx26. Two of the mutations, D50N and G12R, produced large hemichannel currents that increased with cell depolarization and failed to induce any gap-junctional conductance between paired cells. N14K also showed abnormal hemichannel activity that was activated at positive voltages, in addition to producing robust junctional conductance in cell pairs. The voltage-gating sensitivity of junctions formed by N14K channels was greatly reduced compared to wild-type Cx26. The results for the final mutation tested, S17F, differed from both the other mutations and wild-type Cx26. S17F expression induced neither hemichannel currents nor gap-junctional conductance. When cultured in solutions with higher extracellular Ca^{2+} concentrations, all three of the hemichannel forming mutations had reduced levels of activity and increased cell survival. Three of the four KID mutations tested demonstrated significantly increased hemichannel activity compared to the wild-type protein. Taken together with the aforementioned G45E and A40V mutations, increased hemichannel activity appears to be a common feature among GJB2 mutations responsible for KID/HID syndrome.

RESULTS

Gap junction hemichannel currents in single *Xenopus* oocytes

The GJB2 mutations G12R, N14K, S17F, and D50N are the result of single amino-acid substitutions in the N terminus and first extracellular loop Cx26 and are associated with KID/HID syndrome. To assess the functionality of these mutations, wild type, G12R, N14K, S17F, and D50N-Cx26 proteins were expressed in *Xenopus* oocytes. Single cells were subjected to depolarizing voltage pulses and membrane currents were recorded (Figure 1). Oocytes injected with H_2O showed negligible current flow for voltages from −30 to +60 mV. The hemichannel activity of wild-type Cx26-injected cells was previously reported and was characterized by outward currents that increased with greater depolarization (Ripps *et al.*, 2004; Gonzalez *et al.*, 2006; Gerido *et al.*, 2007). Three of the KID mutants, G12R, N14K, and D50N, all showed a significant increase in this outward current when compared to the either H_2O or Cx26-injected cells. This increased membrane current is associated with a reduction in cell membrane resistance and suggests the presence of hemichannels. Conversely, the S17F mutant showed a reduction in membrane current when compared to Cx26-injected cells, and S17F-injected cells were similar to H_2O-injected-negative control cells. This suggested that G12R, N14K, and D50N mutants induced aberrant hemichannel activity, whereas S17F mutants completely eliminated normal hemichannel activity.

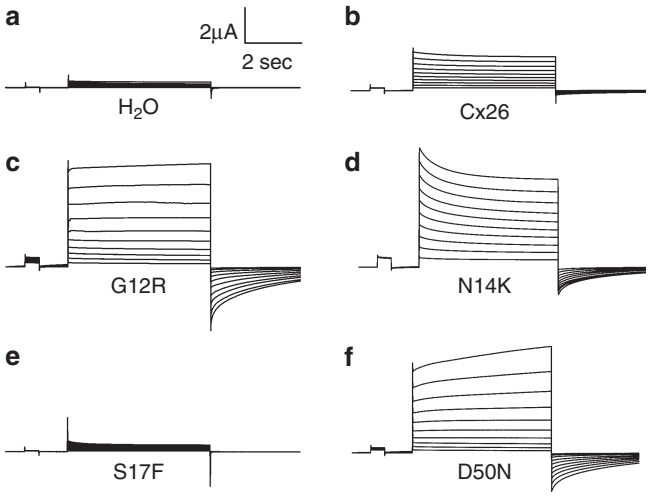

Figure 1. Hemichannel currents recorded from *Xenopus* oocytes. Cells were held at a potential of −40 mV and then membrane currents were recorded at pulses between −30 and +60 mV in 10 mV steps. (**a**) H_2O-injected cells displayed small currents at all potentials. Cells injected with Cx26 (**b**), G12R (**c**), N14K (**d**), and D50N (**f**) displayed hemichannel currents with different magnitudes. S17F cells (**e**) had a negligible current at all voltages recorded.

Mean steady-state currents were plotted as a function of membrane potential to quantify the hemichannel currents (Figure 2). Control cells injected with H_2O showed negligible currents at all tested voltages. Wild-type Cx26-injected cells displayed larger outward currents than H_2O-injected cells that increased at greater depolarizing voltages. At the highest voltage tested, wild-type cells showed a maximum current more than 17 times greater than the control cells (+60 mV, <0.05, Student's *t*-test). The G12R-, N14K-, and D50N-expressing cells produced large outward currents at all voltages tested. At +60 mV, these three mutations exhibited

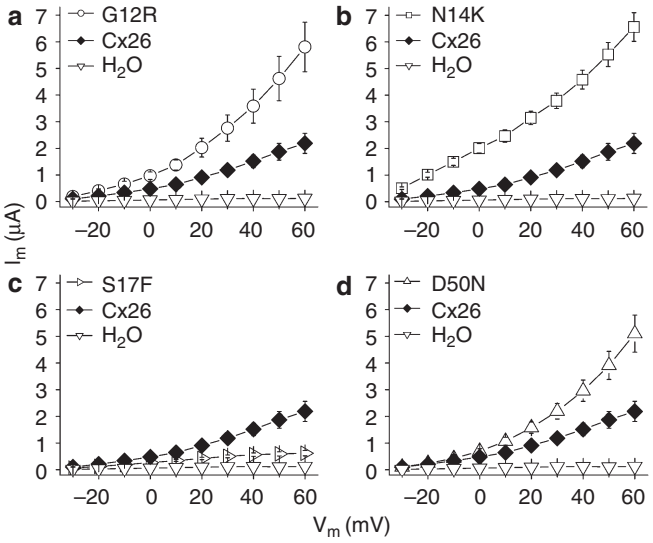

Figure 2. Current-voltage relationship of the wild-type and mutant hemichannels. Cells expressing each mutation were plotted along with H_2O ($n=10$, ▽) and Cx26 ($n=8$, ◆)-injected cells to give a comparison of hemichannel activity. H_2O-injected cells displayed negligible currents at all voltages tested. Cells injected with (**a**) G12R ($n=7$, ○), (**b**) N14K ($n=9$, □), and (**d**) D50N ($n=12$, △) all had currents that were similar to Cx26 at lower voltages but became dramatically larger than Cx26 at increasingly positive potentials. Oocytes injected with (**c**) S17F ($n=11$, ▷) were similar to H_2O-injected cells and displayed a relative lack of current at all voltages tested.

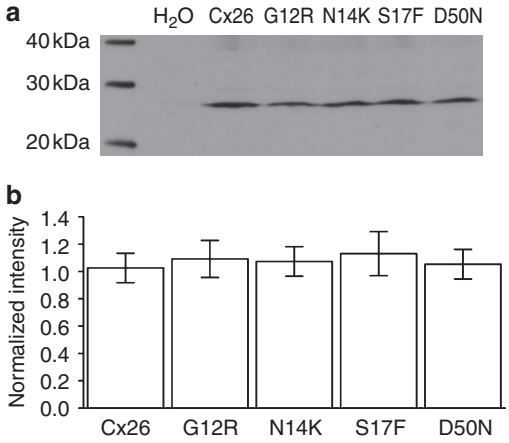

Figure 3. Western blot analysis of protein content from *Xenopus* oocytes. The expression level of each mutation (G12R, N14K, S17F, and D50N) was similar to Cx26. (**a**) Membrane extracts were obtained from an equal number of cells and stained with Cx26 antibodies. H_2O-injected cells were used as a negative control. Cx26, G12R, N14K, S17F, and D50N were seen in their corresponding lanes and in relatively equal amounts. (**b**) The expression levels were tested via densitometry ($n=3$) and were found to be equal for all mutations and wild type ($P>0.05$). Data are means ± SE.

currents that were approximately three times larger than wild type and more than 40 times larger than control cells, differences that were statistically significant (<0.05, one-way analysis of variance). This change represents a difference in membrane conductance associated with each mutation that could be attributed to increased hemichannel activity. Conversely, expression of the S17F mutation in cells caused a significant reduction of current compared to wild-type cells and closely mimicked control cells across all voltages. The introduction of this mutation can be attributed to a reduction in hemichannel activity at increased membrane potentials.

The hemichannel currents recorded from cells expressing the four KID-associated mutations were dramatically different from the wild-type currents. This could have been due to changes in relative quantities of the protein that was produced by the cell or due to a change in activity of the hemichannel. To draw a distinction between these two possibilities, we quantified the amount of protein expressed in the *Xenopus* oocytes by western blot analysis (Figure 3). The band density for each mutation mimicked that of the wild-type expression, with an intensity normalized to wild type of close to 1 for all mutations. This showed that the alterations in current in the hemichannels were not the result of a change in total connexin protein levels.

Cells expressing KID mutations experienced Ca^{2+}-dependent cell death

Cells expressing the G45E and A40V mutations associated with KID syndrome in the Cx26 gene have been shown to cause an increased rate of cell death (Montgomery *et al.*, 2004; Stong *et al.*, 2006; Gerido *et al.*, 2007). Elevated extracellular Ca^{2+} levels are known to inhibit connexin hemichannels (Ebihara and Steiner, 1993) and prolonged the lifespan of G45E-expressing cells (Stong *et al.*, 2006; Gerido *et al.*, 2007). Cells expressing G12R, N14K, S17F, and D50N mutations were incubated in either Ca^{2+}-free modified Barth's medium (MB) solution, or 4 mM Ca^{2+} MB solution immediately after injection with cRNA. Wild-type Cx26 and H_2O-injected cells were incubated as controls. The effects of Ca^{2+} on the cell viability depended on the expressed mutation (Figure 4). There was no apparent difference between cells incubated in high Ca^{2+} or no Ca^{2+} for conditions with wild-type levels of hemichannel activity or lower (H_2O control, Cx26 wild-type, and S17F). These cells were healthy upon visual inspection and showed no signs of cell death after being incubated in media with or without Ca^{2+}. Incubation in media with no Ca^{2+} had a profound effect for cells expressing G12R, N14K, and D50N. The membranes of these cells exhibited blebbing and ooplasm began leaking from the cells within 8–10 hours (Figure 4 top). Typically, G12R-, N14K-, and D50N-expressing cells would undergo lysis and cell death within 24 hours. When G12R, N14K, and D50N were expressed in elevated 4 mM Ca^{2+}, the cells were rescued and the membrane integrity was preserved (Figure 4 bottom).

To determine if the change in the observed rates of cell death in different Ca^{2+} concentrations were statistically significant, cell viability was scored by counting the number of cells with visible blebbing every hour between 12 and 24 hours post cRNA injection. Cells expressing wild type or S17F cRNA showed little variation between 0 and 4 mM Ca^{2+} media (Figure 5a and b). Oocytes injected with G12R, N14K, and D50N showed very different rates between 0 and 4 mM

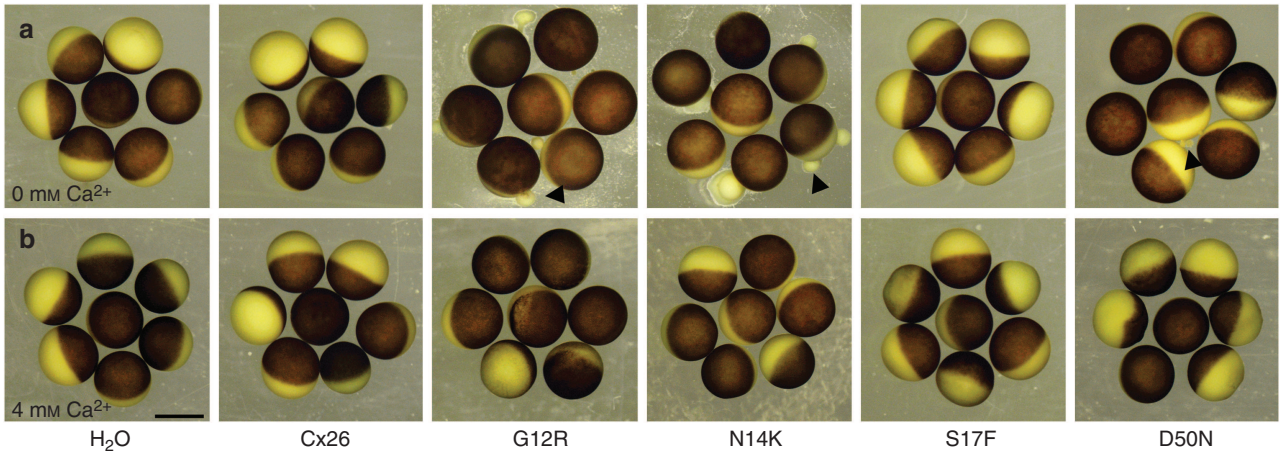

Figure 4. Hemichannel activity-dependent cell death. (**a**) Cells were injected with either H_2O, Cx26, G12R, N14K, S17F, or D50N and incubated in MB solution overnight. Cells injected with H_2O and Cx26 wild type remained viable and intact. Mutations that caused hemichannel activity (G12R, N14K, and D50N) displayed obvious blebbing and an increased rate of cell death compared to Cx26 cells. The S17F mutation that lacked hemichannel activity did not experience the increased rate of cell death. (**b**) Injected cells were incubated in 4 mM Ca^{2+} MB solution overnight. The increased rate of cell death and physical deformation of the membrane experienced by mutations with active hemichannels was rescued by elevated Ca^{2+}. Scale bar = 1 mm.

Ca^{2+}. When incubated in 0 mM Ca^{2+}, these three mutations were statistically different ($P<0.05$, Student's *t*-test) from wild type after 24 hours, whereas S17F-injected oocytes were not ($P>0.05$, Student's *t*-test, Figure 5c). This confirms the observation that cells expressing G12R, N14K, and D50N mutations died at a significantly faster rate than their wild-type counterparts. In contrast, rates of death for S17F-injected oocytes were indistinguishable from wild type. When all cells are incubated in 4 mM Ca^{2+} instead of 0 mM Ca^{2+}, all of the four mutations displayed normal rates of cell death.

Abnormal hemichannel activity was suppressed by extracellular Ca^{2+}

Cells expressing KID mutations that resulted in abnormal hemichannel activity also experienced increased cell death in the absence of elevated extracellular Ca^{2+}. This led us to test whether the addition of extracellular Ca^{2+} that rescued the cells was also blocking the aberrant hemichannel activity of G12R, N14K, and D50N. To assess this, currents were recorded for cells in 0, 1, 2, and 4 mM Ca^{2+} containing MB solutions (Figure 6). Cells containing mutant Cx26 G12R (Figure 6a), N14K (Figure 6b), and D50N (Figure 6c) proteins showed large outward currents in 0 mM Ca^{2+} solutions as documented earlier. The substitution of 1 mM Ca^{2+} led to a significant reduction in membrane currents ($P<0.05$) but did not display a total reduction in outward current. The aberrant hemichannel currents produced by the mutated proteins in 2 and 4 mM Ca^{2+} continued to decrease. The currents were significantly reduced in a concentration-dependent manner, but each mutation showed a different sensitivity to extracellular Ca^{2+} (Figure 6d). This variation in sensitivity is presumably due to the differential effect of each mutation on channel function. However, the variation does not change the phenotype. The mutations responsible for larger aberrant hemichannels still showed increases in cell survivability and decreases in hemichannel currents in higher levels of extracellular Ca^{2+}. The role of hemichannels in cell death seems to be a common feature of Cx26 mutations associated with KID syndrome.

Gap junctions in paired *Xenopus* oocytes

The rescue of cells expressing G12R, N14K, and D50N proteins by elevated Ca^{2+} allowed us to test whether any of our mutations created fully functional intercellular channels using dual whole-cell voltage clamp in paired oocytes (Figure 7). Cells injected with the cRNAs for G12R, N14K, S17F, D50N, or wild-type Cx26 were incubated and paired in 4 mM Ca^{2+}. Water-injected cells were used as a negative control. Cell pairs expressing wild-type Cx26 proteins showed junctional conductances that were 12-fold higher than those for control pairs. Oocyte pairs for G12R, S17F, and D50N showed conductances that were significantly lower than wild-type pairs ($P<0.05$) and were tantamount to control pairs. This suggested the lack of properly functioning gap junctions for these mutations. It has previously been shown by dye transfer assay that S17F showed no gap-junctional coupling (Richard *et al.*, 2002). Curiously, pairs of N14K-expressing cells showed a junctional conductance that was significantly higher than negative controls ($P<0.05$) and indistinguishable from wild-type values.

The formation of gap junction channels by N14K allowed for analysis of the voltage-gating properties. Oocyte pairs expressing N14K showed an apparent loss of the voltage gating seen in their wild-type counterparts. A common feature of wild-type Cx26 traces was the asymmetric nature of decay at higher voltages that was not seen in N14K cell pairs (Figure 8a and b). The steady-state conductance values were normalized, plotted against transjunctional voltage, and fit to a Boltzmann equation (Figure 8c). The complete loss of voltage gating can clearly be seen by the linearity of the N14K data that has a value of unity at all voltages tested and a slope near zero. This apparent difference can be attributed to the N14K mutation and may be part of observed variation in KID phenotype for individuals with this mutation.

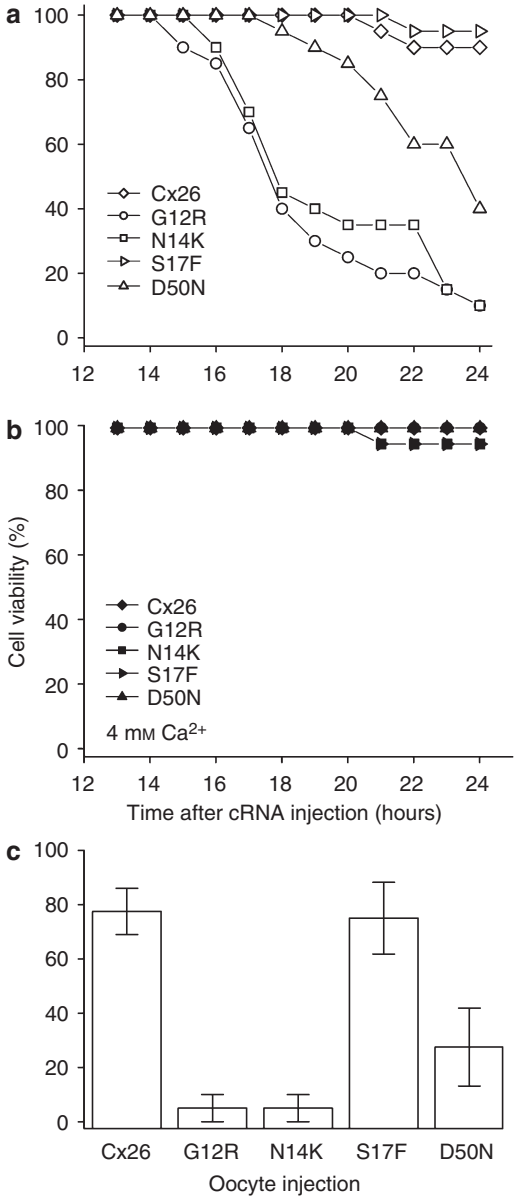

Figure 5. Viability of Cx26 wild-type and mutant expressing cells. (**a**) Cells in 0 mM Ca^{2+} media were scored for cell viability based on the appearance of blebbing. Cells were injected with wild-type Cx26, G12R, N14K, S17F, or D50N cRNA and monitored for 24 hours. These data are based on 20 injected cells per experimental condition. (**b**) Equal numbers of cells expressing the same cRNAs were incubated in 4 mM Ca^{2+} media overnight and scored in the same fashion. (**c**) Cell viability at 24 hours post-injection for all five conditions. The G12R-, N14K-, and D50N-injected cells are statistically different ($P<0.05$, Student's *t*-test) from wild-type-injected cells. Cells injected with S17F were not statistically different from wild type. Data are the mean ± SE from four experiments.

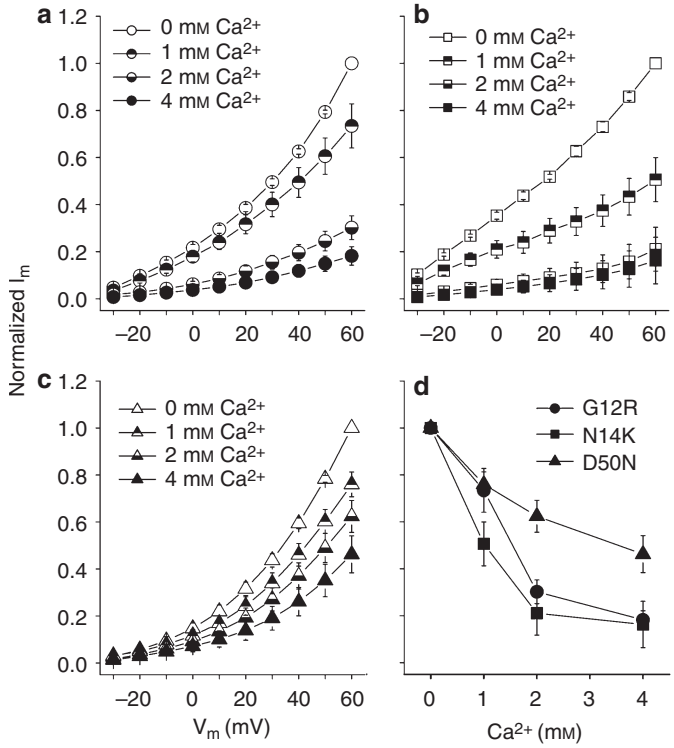

Figure 6. Current–voltage relationships of cells recorded in MB with 0, 1, 2, or 4 mM Ca^{2+} (open, top closed, bottom closed, and completely closed, respectively). Only cells that expressed hemichannels were recorded. (**a**–**c**) Cells were clamped at −40 mV and then tested with pulses from −30 to +60 mV via +10 mV steps. G12R (○), N14K (□), and D50N (△) mutations caused hemichannel activity that increased at positive potentials. The magnitude of hemichannel current was reduced at all potentials as the extracellular concentration of Ca^{2+} increased. (**d**) Currents for each mutation were normalized for steady-state maximal values at each concentration and plotted against the concentration of extracellular Ca^{2+}. There was a distinct difference in the degree and rate of current reduction induced by Ca^{2+}.

DISCUSSION

The appearance of KID syndrome is marked by syndromic deafness and associated skin diseases. Mutations causing nonsyndromic deafness are found throughout the GJB2 protein, but KID syndrome variants are restricted to the N terminus and first extracellular loop. It was previously shown that the KID mutations G45E and A40V resulted in increased hemichannel activity (Montgomery *et al.*, 2004; Gerido *et al.*, 2007). The increased hemichannel currents caused cell death that could be blocked through the addition of extracellular Ca^{2+}. In this study, we examined the behavior of four additional GJB2 mutations associated with SNHL and skin disorders. The G12R, N14K, and D50N mutations led to increased hemichannel activity and cell death. The S17F mutation produced a distinct loss of hemichannel activity altogether, with no cellular lethality. The cell death phenotype of G12R, N14K, and D50N could be rescued through the addition of extracellular Ca^{2+}. These findings are consistent with previous studies describing hemichannel activity associated with Cx26 and suggest a common characteristic among the KID-associated mutations (Montgomery *et al.*, 2004; Stong *et al.*, 2006; Gerido *et al.*, 2007).

The most commonly occurring KID mutation analyzed in this paper is D50N. Reported cases display profound SNHL, photophobia, keratitis, and associated skin disorders (Richard *et al.*, 2002; van Steensel *et al.*, 2002; Mazereeuw-Hautier *et al.*, 2007). The recorded properties of D50N and G12R

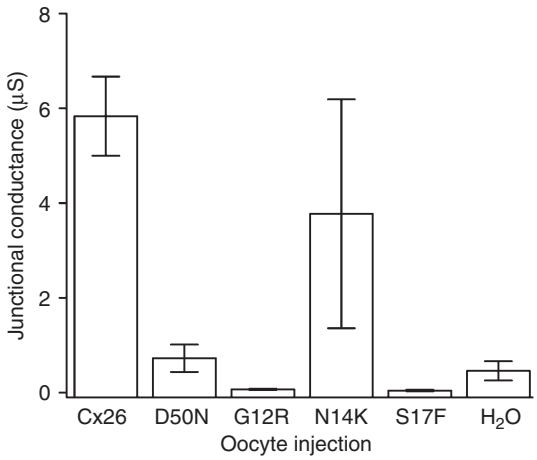

Figure 7. Comparison of junctional conductances recorded from paired *Xenopus* oocytes via dual whole-cell voltage clamp. Pairs of cells expressing Cx26 ($n=43$), D50N ($n=17$), G12R ($n=12$), N14K ($n=19$), S17F ($n=22$), and H_2O ($n=41$) were clamped and held at −40 mV. One cell of the pair was subjected to a voltage pulse whereas the other cell was held constant. The junctional current between cells was recorded and divided by the voltage step to calculate junctional conductance. N14K was the only expressed mutation with a conductance greater than that of H_2O cells. Oocytes with Cx26 and N14K produced a similar junctional conductance. Data are means ± SE.

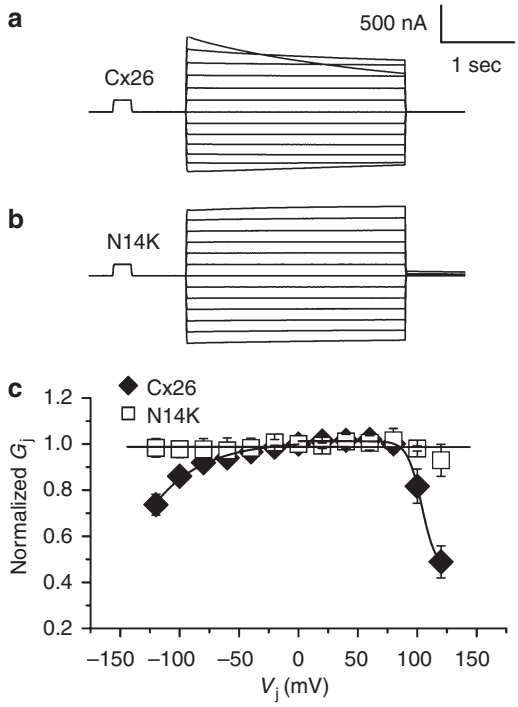

Figure 8. Properties of Cx26 and N14K intercellular junctions. (**a**) Cx26 gap junctions displayed an asymmetric decay in junctional current at transjunctional potentials ⩾ ± 100 mV. (**b**) Gap junctions from pairs of N14K-expressing cells showed a complete loss of voltage sensitivity. (**c**) When normalized junctional conductance was plotted against transjunctional potential, the slope of the line produced by N14K pairs was zero. The Cx26 gap-junctional data could be fit to a Boltzmann equation.

agreed with the theory that KID mutations displayed aberrant hemichannel activity and both mutations failed to induce electrical coupling between paired cells. The cellular death observed in these cases could be rescued by introduction of Ca^{2+} to the extracellular media during incubation. However, the main difference between the two mutations was an apparent change in their sensitivity to the concentration of Ca^{2+}. Hemichannel activity in D50N was less responsive to changes in the extracellular concentration. The response of G12R was quicker and more complete. Both cell populations could be rescued from cell death, but they showed a different reaction to extracellular Ca^{2+} levels. The reduction of D50N currents was smaller than G12R; however, D50N also had a lower magnitude of hemichannel activity in 0 mM Ca^{2+}. Elevation of external calcium reduces the amplitude of hemichannel currents by shifting the voltage activation curve to more positive potentials (Ebihara and Steiner, 1993), such that the mutations with larger hemichannel activity (G12R and N14K) may reflect different activation voltages and experience a larger reduction in current. The underlying cause remains unknown, but may be attributed to the location of the mutations relative to the membrane. The G12R and N14K mutations are bathed in the intracellular solution and D50N is found on the first extracellular loop.

The reported case of N14K was found to have SNHL similar to all of the other mutations reported (van Steensel *et al.*, 2004). However, the patient bearing this mutation was described as having a phenotype more similar to Clouston syndrome (caused by mutations in GJB6) than KID syndrome due to the lack of keratitis and overall mild-associated skin conditions. These observations were consistent with our functional data. The mutant channels led to cell death and elevated hemichannel activity similar to other KID-associated mutations in addition to the formation of complete gap junctions with a conductance similar to wild-type channels. The difference between N14K channels and Cx26 wild-type gap junctions was the complete loss of voltage-dependent gating. The N terminus has been shown to be crucial for voltage-gating properties of channels (Barrio *et al.*, 1991; Oh *et al.*, 1999). It was also reported that the N terminus of Cx26 has a region of flexibility around the first 12–14 amino-acid residues that is important to cellular function (Arita *et al.*, 2006). The loss of voltage gating seen for N14K also suggests that this residue plays a key role in voltage gating. Although several KID mutations have shown no electrical coupling between cells, G45E cells were coupled and the resulting channels demonstrated an increase in voltage sensitivity (Gerido *et al.*, 2007). This suggests that KID mutations that form gap junction channels have reduced conductance at modest transjunctional potentials. The relative loss of conductance compared to wild type could be another property shared by KID mutations. The lack of voltage sensitivity seen by N14K cells may be responsible for causing a phenotype closer to Clouston syndrome by producing conductances across all transjunctional voltages.

One of the most severe phenotypes observed in patients was due to S17F mutation. It has been reported that this condition lead to SNHL, visual impairment, and in one case lethal carcinoma of the tongue (Richard *et al.*, 2002; Mazereeuw-Hautier *et al.*, 2007). Oddly enough, this

mutation also had a different phenotype in our results, displaying a complete lack of both gap-junctional coupling and hemichannel activity. It was similar to negative controls in both experimental recordings. It was also reported that S17F showed a complete lack of coupling in HeLa cells via a dye transfer assay with caboxyfluorescein (Richard *et al.*, 2002). This was consistent with our observations that demonstrated the inability of S17F mutant channels to couple cells. These data suggest that S17F may operate by an alternative method of function previously not classified.

After classification of the functional activity of the four mutations analyzed in this paper, we concluded that aberrant hemichannel activity is a common feature among KID-associated mutations. It has been shown that Cx26 is important in keratinocyte growth and differentiation (Kelsell *et al.*, 2001). There seems to be a distinct pathology for syndromic hearing loss and skin-associated disorders. As was displayed with the N14K mutation, a combination of effects can be caused by the dual activity of Cx26 as both an intercellular channel and a hemichannel interacting with the extracellular solution. With the data from G12R, N14K, S17F, A40V, G45E, and D50N mutations of Cx26, one can conclude that the altered hemichannel activity of these mutants is important in cell signaling (Gerido *et al.*, 2007). The mutation of G11R in Cx30 was also reported to produce hemichannel activity and leads to cell death (Essenfelder *et al.*, 2004). This group also showed the association of A88V with induced cell death in *Xenopus* oocytes. Aberrant hemichannel activity and cell death are common features of Cx26 and Cx30 mutations associated with KID syndrome and other epidermal disorders; however, the precise mechanism whereby this may contribute to a loss of cell viability and tissue integrity remains to be elucidated.

MATERIALS AND METHODS

Molecular cloning

Human wild-type Cx26 was cloned into the *Bam*HI restriction site of the pCS2 + expression vector for functional studies in *Xenopus* laevis oocytes (Rouan *et al.*, 2001). DNA primers (Table S1) with *Bam*HI restriction sites (Integrated DNA Technologies, Inc., Coralville, IA) were designed to generate the G12R, N14K, S17F, and D50N mutations by standard PCR mutagenesis (Mese *et al.*, 2004; Gerido *et al.*, 2007). The G12R-, N14K-, and S17F-specific sense primers were paired with a Cx26 wild-type antisense primer and amplified by PCR with conditions of 95 °C for 4 minutes, followed by 25 cycles of 94 °C for 30 seconds, 60 °C for 30 seconds, 72 °C for 45 seconds, and 72 °C for 2 minutes. The D50N mutation was created by the overlap extension method (Horton *et al.*, 1990), using D50N-specific primers in conjunction with Cx26 sense and antisense primers. PCR products were gel purified using the QIAquik gel extraction kit (Qiagen, Valencia, CA), digested with *Bam*HI and cloned into pBlueScript (Stratagene, La Jolla, CA), and sequenced on both strands (GeneWiz North Brunswick, NJ). Mutants with the correct sequence were subcloned into the pCS2 + vector (Turner and Weintraub, 1994).

In vitro transcription, oocyte microinjection, and pairing

Use of frogs was approved by the Institutional Animal Care and Use Committee. Human Cx26, G12R, N14K, S17F, and D50N were linearized using the *Not*I restriction site of pCS2 +, and transcribed using the SP6 mMessage mMachine (Ambion, Austin, TX). Adult *Xenopus* females were anesthetized with ethyl 3-aminobenzoate methanesulfonate, and ovarian lobes were surgically removed and digested for 1.5 hours in a solution containing 50 mg ml^{-1} collagenase B, and 50 mg ml^{-1} hyaluronidase in MB without Ca^{2+}. Stages V–VI oocytes were collected and injected first with 10 ng of antisense *Xenopus* Cx38 oligonucleotide to eliminate endogenous connexins (Barrio *et al.*, 1991; Bruzzone *et al.*, 1993). Antisense oligonucleotide-treated oocytes were then injected with wild-type Cx26, G12R, N14K, S17F, and D50N cRNA transcripts (5 ng per cell), or H_2O as a negative control. cRNA-injected oocytes were then cultured in Ca^{2+}-free MB, or MB with elevated Ca^{2+} (4 mM $CaCl_2$) and cultured until ready for electrophysiological recording or image capture. For measurements of gap-junctional conductance, the vitelline envelopes were removed in a hypertonic solution (200 mM aspartic acid, 10 mM HEPES, 1 mM $MgCl_2$, 10 mM EGTA, and 20 mM KCL at pH 7.4), and the oocytes were manually paired with the vegetal poles apposed in MB with elevated Ca^{2+}.

Electrophysiological hemichannel current recordings

At 8–12 hours after cRNA injection, macroscopic recordings of hemichannel currents were recorded from single *Xenopus* oocytes using a GeneClamp 500 amplifier controlled by a PC-compatible computer through a Digidata 1320 interface (Axon Instruments, Foster City, CA). pClamp 8.0 software (Axon Instruments) was used to program stimulus and data collection paradigms. To obtain hemichannel *I–V* curves, cells were initially clamped at −40 mV and subjected to 5 seconds depolarizing voltage steps ranging from −30 to +60 mV in 10 mV increments. To test the effect of extracellular Ca^{2+} on hemichannel currents, oocytes were switched between MB media without Ca^{2+}, or MB supplemented with elevated Ca^{2+} (1, 2, and 4 mM $CaCl_2$) via a perfusion system that washed 25 ml of solution through the 35 mm dish before recording. Cells were allowed to rest in the new solution for 2–5 minutes before recording.

Dual whole-cell voltage clamp

Gap-junctional coupling between oocyte pairs was measured using the dual whole-cell voltage clamp technique (Spray *et al.*, 1981). Current and voltage electrodes (1.2 mm diameter, omega dot; Glass Company of America, Millville, NJ) were pulled to a resistance of 1–2 MΩ with a horizontal puller (Narishige, Tokyo, Japan) and filled with solution containing 3 M KCl, 10 mM EGTA, and 10 mM HEPES, pH 7.4. Dual voltage clamp experiments were performed using the same amplifier, data acquisition interface, computer, and software used for hemichannel current recordings. For measurements of junctional conductance, both cells in a pair were initially clamped at −40 mV to eliminate any transjunctional potential. One cell was then subjected to alternating pulses of ± 20 mV, whereas the current produced by the change in voltage was recorded in the second cell. The current delivered to the second cell was equal in magnitude to the junctional current, and the junctional conductance was calculated by dividing the measured current by the voltage difference, $G_j = I_j/(V_1 - V_2)$.

To determine voltage-gating properties, transjunctional potentials (V_j) of opposite polarity were generated by hyperpolarizing or depolarizing one cell in 20 mV steps (range, ± 120 mV) while

clamping the second cell at −40 mV. Currents were measured at the end of the voltage pulse, at which time they approached steady state (I_{jss}). Macroscopic conductance (G_{jss}) was calculated by dividing I_{jss} by V_j, normalized to the values determined at ± 20 mV, and plotted against V_j. Data describing the relationship of G_{jss} as a function of V_j were analyzed using Origin 6.1 (Microcal Software, Northampton, MA) and fit to a Boltzmann relation of the form: $G_{jss} = (G_{jmax} - G_{jmin})/1 + \exp(A(V_j - V_0)) = G_{jmin}$, where G_{jss} is the steady-state junctional conductance, G_{jmax} (normalized to unity) is the maximum conductance, G_{jmin} is the residual conductance at large values of V_j, and V_0 is the transjunctional voltage at which $G_{jss} = (G_{jmax} - G_{jmin})/2$. The constant $A = nq/kT$ represents the voltage sensitivity in terms of gating charge as the equivalent number (n) of electron charges (q) moving through the membrane, k is the Boltzmann constant, and T is the absolute temperature.

Preparation of oocyte samples for western blot analysis and quantification

Oocytes used for electrophysiological recording were collected in 2 ml tubes and frozen at −80 °C. Oocytes were homogenized in 1 ml of buffer containing 5 mM Tris, pH 8.0, 5 mM EDTA and protease inhibitors using a series of mechanical passages through needles of diminishing caliber (20, 22, 26 gauge). Extracts were centrifuged at 1,000 *g* at 4 °C for 5 min. The supernatant was then centrifuged at 100,000 *g* at 4 °C for 30 min. Membrane pellets were resuspended in SDS sample buffer (1 µl per oocyte), samples were separated on 15% SDS gels and transferred to nitrocellulose membranes. Blots were blocked with 5% BSA in 1 × phosphate-buffered saline with 0.02% NaN_3 for 1 hour and probed with a polyclonal Cx26 antibody, at a 1:500 dilution (Zymed Laboratories, San Francisco, CA), followed by incubation with alkaline-phosphatase conjugated anti-rabbit secondary antibody (Jackson ImmunoResearch Laboratories, West Grove, PA). Band intensities were quantified using Kodak 1D Image Analysis software (Eastman Kodak, Rochester, NY). Values from three independent experiments were normalized to the mean value of band intensity of the wild-type Cx26 sample.

CONFLICT OF INTEREST

The authors state no conflict of interest.

ACKNOWLEDGMENTS

This work was supported by NIH grants EY13163 and DC06652 (TWW). We thank Dr Gülistan Meşe for critically reading the paper.

SUPPLEMENTARY MATERIAL

Table S1. PCR primers used to generate Cx26 mutations.

REFERENCES

Anand RJ, Hackam DJ (2005) The role of gap junctions in health and disease. *Crit Care Med* 33:S535–8

Arita K, Akiyama M, Aizawa T, Umetsu Y, Segawa I, Goto M *et al.* (2006) A novel N14Y mutation in Connexin26 in keratitis-ichthyosis-deafness syndrome: analyses of altered gap junctional communication and molecular structure of N terminus of mutated Connexin26. *Am J Pathol* 169:416–23

Barrio LC, Suchyna T, Bargiello T, Xu LX, Roginski RS, Bennett MV *et al.* (1991) Gap junctions formed by connexins 26 and 32 alone and in combination are differently affected by applied voltage. *Proc Natl Acad Sci USA* 88:8410–4

Bennett MV, Contreras JE, Bukauskas FF, Saez JC (2003) New roles for astrocytes: gap junction hemichannels have something to communicate. *Trends Neurosci* 26:610–7

Bruzzone R, Haefliger JA, Gimlich RL, Paul DL (1993) Connexin40, a component of gap junctions in vascular endothelium, is restricted in its ability to interact with other connexins. *Mol Biol Cell* 4:7–20

Bruzzone R, Veronesi V, Gomes D, Bicego M, Duval N, Marlin S *et al.* (2003) Loss-of-function and residual channel activity of connexin26 mutations associated with non-syndromic deafness. *FEBS Lett* 533:79–88

Ebihara L, Steiner E (1993) Properties of a nonjunctional current expressed from a rat connexin46 cDNA in *Xenopus* oocytes. *J Gen Physiol* 102:59–74

Essenfelder GM, Bruzzone R, Lamartine J, Charollais A, Blanchet-Bardon C, Barbe MT *et al.* (2004) Connexin30 mutations responsible for hidrotic ectodermal dysplasia cause abnormal hemichannel activity. *Hum Mol Genet* 13:1703–14

Gerido DA, DeRosa AM, Richard G, White TW (2007) Aberrant hemichannel properties of Cx26 mutations causing skin disease and deafness. *Am J Physiol Cell Physiol* 293:C337–45

Gerido DA, White TW (2004) Connexin disorders of the ear, skin, and lens. *Biochim Biophys Acta* 1662:159–70

Gonzalez D, Gomez-Hernandez JM, Barrio LC (2006) Species specificity of mammalian connexin-26 to form open voltage-gated hemichannels. *FASEB J* 20:2329–38

Goodenough DA, Paul DL (2003) Beyond the gap: functions of unpaired connexon channels. *Nat Rev Mol Cell Biol* 4:285–94

Harris AL (2001) Emerging issues of connexin channels: biophysics fills the gap. *Q Rev Biophys* 34:325–472

Horton RM, Cai ZL, Ho SN, Pease LR (1990) Gene splicing by overlap extension: tailor-made genes using the polymerase chain reaction. *Biotechniques* 8:528–35

Janecke AR, Hennies HC, Gunther B, Gansl G, Smolle J, Messmer EM *et al.* (2005) GJB2 mutations in keratitis-ichthyosis-deafness syndrome including its fatal form. *Am J Med Genet A* 133:128–31

Jonard L, Feldmann D, Parsy C, Freitag S, Sinico M, Koval C *et al.* (2008) A familial case of keratitis-ichthyosis-deafness (KID) syndrome with the GJB2 mutation G45E. *Eur J Med Genet* 51:35–43

Kelsell DP, Dunlop J, Hodgins MB (2001) Human diseases: clues to cracking the connexin code? *Trends Cell Biol* 11:2–6

Lai-Cheong JE, Arita K, McGrath JA (2007) Genetic diseases of junctions. *J Invest Dermatol* 127:2713–25

Mazereeuw-Hautier J, Bitoun E, Chevrant-Breton J, Man SY, Bodemer C, Prins C *et al.* (2007) Keratitis-ichthyosis-deafness syndrome: disease expression and spectrum of connexin 26 (GJB2) mutations in 14 patients. *Br J Dermatol* 156:1015–9

Mese G, Londin E, Mui R, Brink PR, White TW (2004) Altered gating properties of functional Cx26 mutants associated with recessive non-syndromic hearing loss. *Hum Genet* 115:191–9

Mese G, Richard G, White TW (2007) Gap junctions: basic structure and function. *J Invest Dermatol* 127:2516–24

Montgomery JR, White TW, Martin BL, Turner ML, Holland SM (2004) A novel connexin 26 gene mutation associated with features of the keratitis-ichthyosis-deafness syndrome and the follicular occlusion triad. *J Am Acad Dermatol* 51:377–82

Oh S, Rubin JB, Bennett MV, Verselis VK, Bargiello TA (1999) Molecular determinants of electrical rectification of single channel conductance in gap junctions formed by connexins 26 and 32. *J Gen Physiol* 114:339–64

Petit C (2006) From deafness genes to hearing mechanisms: harmony and counterpoint. *Trends Mol Med* 12:57–64

Petit C, Levilliers J, Hardelin JP (2001) Molecular genetics of hearing loss. *Annu Rev Genet* 35:589–646

Richard G (2005) Connexin disorders of the skin. *Clin Dermatol* 23:23–32

Richard G, Rouan F, Willoughby CE, Brown N, Chung P, Ryynanen M *et al.* (2002) Missense mutations in GJB2 encoding connexin-26 cause the ectodermal dysplasia keratitis-ichthyosis-deafness syndrome. *Am J Hum Genet* 70:1341–8

Ripps H, Qian H, Zakevicius J (2004) Properties of connexin26 hemichannels expressed in *Xenopus* oocytes. *Cell Mol Neurobiol* 24:647–65

Rouan F, White TW, Brown N, Taylor AM, Lucke TW, Paul DL *et al.* (2001) *trans*-Dominant inhibition of connexin-43 by mutant connexin-26: implications for dominant connexin disorders affecting epidermal differentiation. *J Cell Sci* 114:2105–13

Saez JC, Retamal MA, Basilio D, Bukauskas FF, Bennett MV (2005) Connexin-based gap junction hemichannels: gating mechanisms. *Biochim Biophys Acta* 1711:215–24

Spray DC, Harris AL, Bennett MV (1981) Equilibrium properties of a voltage-dependent junctional conductance. *J Gen Physiol* 77:77–93

Stong BC, Chang Q, Ahmad S, Lin X (2006) A novel mechanism for connexin 26 mutation linked deafness: cell death caused by leaky gap junction hemichannels. *Laryngoscope* 116:2205–10

Turner DL, Weintraub H (1994) Expression of achaete-scute homolog 3 in *Xenopus* embryos converts ectodermal cells to a neural fate. *Genes Dev* 8:1434–47

van Geel M, van Steensel MA, Kuster W, Hennies HC, Happle R, Steijlen PM *et al.* (2002) HID and KID syndromes are associated with the same connexin 26 mutation. *Br J Dermatol* 146:938–42

van Steensel MA, Steijlen PM, Bladergroen RS, Hoefsloot EH, Ravenswaaij-Arts CM, van Geel M (2004) A phenotype resembling the Clouston syndrome with deafness is associated with a novel missense GJB2 mutation. *J Invest Dermatol* 123:291–3

van Steensel MA, van Geel M, Nahuys M, Smitt JH, Steijlen PM (2002) A novel connexin 26 mutation in a patient diagnosed with keratitis-ichthyosis-deafness syndrome. *J Invest Dermatol* 118:724–7

Wei CJ, Xu X, Lo CW (2004) Connexins and cell signaling in development and disease. *Annu Rev Cell Dev Biol* 20:811–38

White TW (2000) Functional analysis of human Cx26 mutations associated with deafness. *Brain Res Brain Res Rev* 32:181–3

White TW, Paul DL (1999) Genetic diseases and gene knockouts reveal diverse connexin functions. *Annu Rev Physiol* 61:283–310

Zhao HB, Kikuchi T, Ngezahayo A, White TW (2006) Gap junctions and cochlear homeostasis. *J Membr Biol* 209:177–86